Optimal use of EEG recordings to target active brain areas with transcranial electrical stimulation

Jacek P. Dmochowski[a,*], **Laurent Koessler**[b], **Anthony M. Norcia**[c], **Marom Bikson**[d], **Lucas C. Parra**[d]

[a]Department of Biomedical Engineering, Steinman Hall 460 City College of New York, New York, NY 10031, USA

[b]CNRS - University of Lorraine, France

[c]Stanford University, USA

[d]City College of New York, USA

Abstract

To demonstrate causal relationships between brain and behavior, investigators would like to guide brain stimulation using measurements of neural activity. Particularly promising in this context are electroencephalography (EEG) and transcranial electrical stimulation (TES), as they are linked by a reciprocity principle which, despite being known for decades, has not led to a formalism for relating EEG recordings to optimal stimulation parameters. Here we derive a closed-form expression for the TES configuration that optimally stimulates (i.e., targets) the sources of recorded EEG, without making assumptions about source location or distribution. We also derive a duality between TES targeting and EEG source localization, and demonstrate that in cases where source localization fails, so does the proposed targeting. Numerical simulations with multiple head models confirm these theoretical predictions and quantify the achieved stimulation in terms of focality and intensity. We show that constraining the stimulation currents automatically selects optimal montages that involve only a few (4–7) electrodes, with only incremental loss in performance when targeting focal activations. The proposed technique allows brain scientists and clinicians to rationally target the sources of observed EEG and thus overcomes a major obstacle to the realization of individualized or closed-loop brain stimulation.

Keywords

EEG; Transcranial direct current stimulation; Transcranial electrical stimulation; Reciprocity; Closed-loop stimulation; Source localization

Introduction

The ability to systematically modify observed patterns of neural activity would be highly beneficial on at least two fronts: in basic neuroscience, mapping out the relationship

*Corresponding author: jdmochowski@ccny.cuny.edu (J.P. Dmochowski).

between structure and function is facilitated by causal manipulations of brain activity. Moreover, techniques supporting target engagement provide novel strategies for treating psychiatric and neurological disorders marked by aberrant neural dynamics (Uhlhaas and Singer, 2006, 2012). An intriguing approach is to combine neuroimaging with brain stimulation (Bestmann and Feredoes, 2013; Bergmann et al., 2016; Siebner et al., 2009). The technical capability to perform integrated stimulation-recording of brain activity exists at a variety of scales: invasive microelectrode arrays (Maynard et al., 1997; Jimbo et al., 2003; Dostrovsky et al., 2000), deep brain stimulation (DBS) (Kent and Grill, 2013; Lempka and McIntyre, 2013; Rosin et al., 2011), depth electrodes (Rosenberg et al., 2009), cortical surface electrode arrays (Trebuchon et al., 2012), brain machine interfaces (Guggenmos et al., 2013), and non-invasive scalp electrode arrays that are commonly used in human neuroscience (Thut et al., 2005; Faria et al., 2012; Fernández-Corazza et al., 2016; Wagner et al., 2016b). However, lacking is a general formalism for how to select stimulation parameters given observations of neural activity.

One particularly compelling combination is electroencephalography (EEG) with transcranial electrical stimulation (TES), mirror-symmetric processes related by the long-standing reciprocity principle introduced by Helmholtz (1853). Simply stated, the electrical path from a neural source to a (recording) electrode is equivalent to the electrical path from the (now stimulating) electrode to the location of the neural source (Rush and Driscoll, 1969). Intuition suggests that reciprocity should allow one to leverage the information carried by EEG signals to guide the parameters of the TES. Indeed, recent work has proposed ad hoc rules for distilling EEG measurements to TES configurations ("montages") (Fernández-Corazza et al., 2016; Cancelli et al., 2016). However, these initial efforts have not realized the multi-dimensional nature of the reciprocity principle, and thus have failed to overcome the spatial blurring that results from naive implementations of reciprocal stimulation.

Here we develop a general formalism for combined EEG-TES, focusing on the problem of how to select the applied TES currents such that the source of an EEG activation is targeted by the stimulation. By formulating both EEG and TES as linear systems linked by a common transfer matrix, we derive a closed-form expression for the TES electrode configuration ("montage") that generates an electric field most closely matched to the activation pattern. Importantly, we show that source localization of the targeted activation is not required, and that EEG sources may be stimulated using only their projections on the scalp. However, we also derive a duality between EEG localization and TES targeting, showing that the inherent limitations of localization are shared by targeting. In order to guarantee "safe" (i.e., current-limited) and feasible montages, we propose to constrain the L^1 norm of the reciprocal TES solution, and provide a fast iterative scheme to achieve this.

In order to test the proposed approach, we conduct numerical simulations using two magnetic resonance imaging (MRI) based models of the human head. The simulations confirm the main theoretical prediction that in order to target the source of a recorded EEG pattern, the TES currents must be selected as the *spatially decorrelated* vector of measured EEG potentials. The duality between EEG and TES is also validated, and we present a high-noise scenario in which both EEG localization and TES targeting fail. We then demonstrate that the L^1 constrained solution allows for simple montages that

increase stimulation intensity while only sacrificing a modest amount of focality. We show that reciprocal stimulation accounts for varying source orientation, in that both radial and tangential sources are effectively targeted. Finally, we evaluate reciprocal TES when active sources are distributed. In summary, we demonstrate that targeted stimulation of neural sources may be achieved by measuring neural activity at a surface array and using these measurements to design spatially patterned electrical stimulation. This approach has application to both basic neuroscience and clinical interventions using neuromodulation.

Results

TES delivers electric currents to the brain via an array of scalp electrodes, while EEG records voltages on the scalp generated by neural current sources in the brain. The goal of reciprocal TES is to select the stimulation currents on the scalp such that they reproduce the neural current sources in the brain. We provide the mathematical theory to optimally achieve this goal, while deferring proofs to the Methods. To test the theoretical predictions (Figs. 1–3), we employ a simple 3-compartment boundary element model (BEM) of the human head based on a tissue segmentation derived from MRI (see Methods for details). To estimate the performance of reciprocal TES in practice (Figs. 4–7), we make use of a more detailed finite element model (FEM) with 6 compartments that captures idiosyncrasies in human head anatomy (Huang et al., 2015). These head models allowed for the estimation of stimulation currents in the brain as well as simulation of voltage recordings due to neural currents.

EEG lead field and TES forward model are symmetric

Consider an array of N electrodes that is capable of both recording (neurally-generated) electric potentials and stimulating the brain with applied electrical currents. The recorded voltages, denoted by N-dimensional vector V (units of V), are a linear superposition of M neural current source vectors whose activity is represented by 3M-dimensional vector J (units of A·m):

$$V = RJ, \tag{1}$$

where N-by-3M matrix R (units of Ω/m) is the so-called "lead field" matrix (Sarvas, 1987; Hämäläinen and Ilmoniemi, 1994) that quantifies the voltages generated on the scalp by unit currents at various source locations and orientations in the brain ($M \gg N$). One example is given in Fig. 1A, which shows a localized source of activity on the cortical surface. Note that the voltage recordings on the scalp are blurred due to volume conduction. The stimulation currents applied to the electrode array, denoted by N-dimensional vector I (units of A), generate an electric field E (units of V/m) inside the brain:

$$E = SI, \tag{2}$$

where E is a vector of dimension 3M that spans the three Cartesian dimensions and matrix S (units of Ω/m) is the 3M-by-N "forward model" (Dmochowski et al., 2011) that quantifies the electric field generated in the brain for a unit current applied to each of the stimulation

electrodes. In this multiple electrode context, reciprocity leads to a symmetry relationship among R and S:

$$R^T = S, \tag{3}$$

where ^{T} denotes matrix transposition. This formulation of reciprocity is novel in that it describes the relationship between *multiple* neural sources and *multiple* electrode pairs. Reciprocity for individual sources and a single pair of recording electrodes in a non-uniform medium such as the brain has been known for decades (Rush and Driscoll, 1969), and linear superposition of multiple sources has been previously leveraged for current flow modeling (Hallez et al., 2007; Huang et al., 2015; Wagner et al., 2016b), but a compact formulation as in Equation (3) was lacking. We provide a derivation for this multi-dimensional reciprocity in the Methods. In the next section, we exploit multi-dimensional reciprocity to, for the first time, selectively target active neural sources with appropriately tuned stimulation currents.

Reciprocal TES inverts the spatial blurring of EEG potentials

To modulate the neural activity underlying the EEG, we propose to recreate with TES an electric field that matches the neural source distribution. In mathematical terms, an ideal outcome is thus $E = cJ$, where c is a constant (units of Ω/m^2) that relates the magnitude of neural activation (measured in A·m) to the strength of the desired electric field (measured in V/m). The selection of stimulation currents to achieve this goal can be formulated as a convex optimization problem:

$$\begin{aligned} I^* &= \arg\ \min_I\ \|E - cJ\|^2 \\ &= c\,(RR^T)^{-1}V. \end{aligned} \tag{4}$$

The result of (4) states that to modulate the sources of an observed EEG pattern V, one should apply TES currents according to $c(RR^T)^{-1}V$, where the matrix inverse compensates for the spatial mixing due to lead fields R and exists provided that the columns of R^T are linearly independent. This solution is in contrast to a "naive" reciprocity approach, which simply applies currents with the same spatial pattern as the recorded voltage distribution: $I^* \propto V$ (Cancelli et al., 2016) and does not decorrelate the recorded voltages. Note that the ability of optimal reciprocity (4) to account for volume conduction is predicated on the availability of the lead field matrix R, which conveys the set of *possible* source locations (e.g., all cortical locations).

To compare the results of optimal reciprocity with the naive approach, we simulated activation of a patch of cortical tissue (bounded by a sphere of 1 cm radius) in the right frontal cortex (Fig. 1A, left). Each source was oriented perpendicular to the cortical sheet, following the notion that pyramidal neurons are the primary source of the EEG (Nunez and Srinivasan, 2006). The resulting scalp potentials were marked by a positivity at right frontocentral electrodes and a diffuse negativity at surrounding sites (Fig. 1A, right). This EEG pattern was then used as an input into two forms of TES aimed at stimulating the activation region: the naive reciprocity approach ($I^* \propto V$) and optimal reciprocity according to (4). The electric field resulting from the naive approach (Fig. 1B, left) had a large

magnitude of 0.25 V/m in the neural activation region; however, the field pattern was excessively diffuse. The focality of the electric field, quantified as the radius at which field magnitude drops by half, was 8.2 cm (Fig. 1B, left). Optimal reciprocity resulted in a focused electric field that still strongly activated the target region (0.16 V/m), while exhibiting a more compact stimulation radius of 4.0 cm (Fig. 1C, left). The resulting field did not exactly match the original neural source distribution because the scalp potentials were only measured at a limited number of locations (i.e., 64). In theory, if voltages could be measured noise-free and with as many electrodes as neural sources, and assuming that the sources perfectly conform to the underlying mixing model (1), one could exactly recreate the distribution.

Note that the reciprocal TES montage consisted of both positive and negative stimulation currents in the scalp region marked by positive EEG (Fig. 1C, right). We also mention that the result of (4) corresponds to "anodal" stimulation: that is, direct currents I will depolarize neurons oriented perpendicular to the cortical surface. If one instead seeks to hyperpolarize such cells ("cathodal" stimulation), the stimulation currents take the form $I^* = -c(RR^T)^{-1} V$.

EEG localization and TES targeting are dual problems

Note that the neural source distribution J does *not* enter the expression for the reciprocal currents I^*: this variable is "absorbed" by the lead field R in the derivation of (4) – see the Methods. This means that in order to reproduce the activity pattern, one need not know the locations of the active sources in the brain, but only their voltage measurements on the scalp. It may thus appear that reciprocity has solved the ill-posed inverse problem inherent to encephalography (Pascual-Marqui, 1999). However, as we show in the Methods section, source localization and reciprocal targeting are actually dual mathematical problems. Specifically, the optimal electric field E^* achieved with reciprocal targeting following (4) is proportional to the conventional minimum-norm estimate of the neural source distribution J^*:

$$J^* = E^*/c.$$ (5)

Importantly, (5) implies that in instances where the minimum-norm source estimate J^* is inaccurate, the electric field E^* generated by reciprocal stimulation will also be misguided.

To examine the duality between source localization and reciprocal targeting, we simulated bilateral activation of the parietal cortex (Fig. 2A) under two distinct noise conditions: spatially white noise was added to the electrodes with a signal-to-noise ratio (SNR) of either 100 or 1. In the low-noise case, the topography of the EEG clearly showed a radially symmetric pattern centered over centroparietal electrodes (Fig. 2B). The TES montage that reciprocated this pattern consisted of a central anode surrounded by four cathodes (Fig. 2C), producing an electric field with an intensity of 0.12 V/m at the activated region and a focality of 3.3 cm (Fig. 2D). We then computed the minimum norm source estimate of the EEG topography. Confirming the theoretical prediction (Eq. (5)), this estimate was found to be perfectly correlated with the electric field generated by reciprocal TES (r=1, Fig. 2E). In the high-noise case, the EEG topography exhibited distortion (Fig. 2F), leading to a

reciprocal TES montage that erroneously recruited bilateral frontal electrodes (Fig. 2G). The electric field produced by this montage "missed" the site of activation and was distributed along the midline (Fig. 2H). Again confirming the theoretical prediction, the minimum-norm estimate of the neural source distribution underlying the distorted EEG pattern was found to be perfectly correlated with this electric field (r=1, Fig. 2I).

Constraining the L^1-norm of reciprocal montages

The magnitudes of I^*, as computed by Eq. (4), may be less or greater than those desired in practice. For example, the presently accepted safety practice for TES is to deliver no more than 2 mA to the head (Brunoni et al., 2012; Bikson et al., 2016). Denoting the limit on current delivered by I_{max} (e.g. 2 mA), safe stimulation corresponds to a constraint on the sum of absolute currents:

$$\|I\|_1 = \sum_n |I_n| < 2I_{max}.$$

(6)

Eq. (6) specifies a constraint on the "L^1 norm" of stimulation currents I. In cases where the unconstrained solution from Eq. (4) violates the inequality, we must somehow adjust I^* to adhere to this safety constraint. The simplest way of achieving this is through a uniform scaling of the elements of I^*:

$$I^*: = \frac{I^*}{\|I^*\|_1}2I_{max}.$$

(7)

However, it is important to note that scaling I^* via (7) does *not* minimize the mean squared error between E and cJ subject to the constraint (6). Therefore, we propose the following constrained optimization problem:

$$I_1^* = \arg\min_I \|E - cJ\|^2 \text{ subject to} \|I\|_1 < 2I_{max}.$$

(8)

Unlike the unconstrained case (4), the optimization problem (8) does not have a closed-form solution. However, a number of algorithms have been proposed in order to numerically solve such L^1-constrained least-squares problems (Tibshirani, 1996). In the Methods, we propose an iterative scheme that converts the (non-differentiable) L^1 constraint to a set of linear constraints that may be iteratively solved using standard numerical packages. The solution to (8) represents the pattern of stimulation currents that best recreates the neural activation while maintaining safe current levels.

To demonstrate the effect of constraining the L^1 norm of the reciprocal TES solution on the achieved stimulation, we performed L^1-constrained reciprocity with $c = 10^{10}\Omega/m^2$ on activations from all sources in the BEM head model (see Methods for details). For each activation, we computed both the optimal (unconstrained) and L^1-constrained reciprocal TES montages. An example activation of the primary visual cortex is depicted in Fig. 3A. In this case, unconstrained reciprocity led to the stimulation currents being distributed over

approximately 8 electrodes, producing an electric field with an intensity of 0.18 V/m at the activation and a focality of 3.3 cm (Fig. 3B). The L^1-constrained montage was limited to 5 active electrodes, and produced a three-fold increase in the mean electric field intensity at the activated region (Fig. 3C, 0.53 V/m), while only suffering a slight reduction in focality (i.e., 3.7 cm). Comparing the focality and intensity of the electric fields produced by both unconstrained and L^1-constrained reciprocity across all activations confirmed that the L^1-constrained solution provided an excellent tradeoff between focality and intensity (unconstrained reciprocity: 0.07 ± 0.05 V/m, 4.5 ± 1.0 cm; L^1-constrained: 0.18 ± 0.17 V/m, 4.6 ± 0.8 cm; Fig. 3D). The difference between unconstrained and L^1 constrained was found to be statistically significant in both focality ($p = 0$ to numerical precision, $N = 15002$, Wilcoxon signed rank test), and intensity ($p = 0$).

In validating the theoretical findings above, we have used a relatively simple BEM model of the head. In the following, we seek to estimate the performance of reciprocal TES in practice. To that end, we employed a more detailed finite element model (FEM) that captured idiosyncrasies in head anatomy (see Methods and Huang et al. (2015)).

Quantifying the tradeoff between focality and intensity

For unconstrained reciprocity (4), the value of c is inconsequential – in practice, the currents will be scaled to the desired level using Eq. (7). However, for L^1-constrained reciprocity (8), the value of c will determine the distribution of the optimal stimulation currents, and consequently, the shape of the electric field. To examine the effect of varying parameter c, we performed L^1-constrained reciprocal stimulation for varying values of parameter c, which relates the strength of the desired electric field E to the magnitude of the neural activation J. We simulated activation of four distinct cortical regions in the FEM: the superior temporal gyrus (STG, Fig. 4A), the dorsolateral prefrontal cortex (DLPFC, Fig. 4B), the superior parietal lobule (SPL, Fig. 4C), and visual area V5 (also known as the middle temporal (MT) visual area, Fig. 4D). Given that the neural sources of EEG have intensities in the order of 1 nm·A (Nunez and Srinivasan, 2006), and that the electric fields produced by TES are in the order of 0.5 V/m (Opitz et al., 2016), the parameter should be selected to be large (i.e., c ranged from 10^8 to $10^{14} \Omega/m^2$). Larger values of c led to higher intensity but lower focality of stimulation at the target (Fig. 4A–D, circle markers). Importantly, the focality-intensity curve increased gradually at low values of c, suggesting that intensity can be substantially increased (i.e., two or three fold) while only sacrificing a modest amount of focality (i.e., 1 or 2 cm). For the example activations here, a good tradeoff between focality and intensity point occurred at $c = 10^{10} \Omega/m^2$ and $c = 10^{11} \Omega/m^2$. In addition to increasing stimulation intensity, larger values of c also produced montages utilizing less active electrodes (represented by color of markers). At $c = 10^{10}$, L^1-constrained montages recruited between 4 and 7 electrodes.

Performance of reciprocal TES as a function of location

In order to quantify the performance of reciprocal TES as a function of target location, we performed L^1-constrained reciprocity with $c = 10^{10} \Omega/m^2$ on activations from all sources in the FEM head model (see Methods for details). We plotted the focality and intensity achieved by L^1-constrained reciprocity on cortex. The focality of stimulation ranged from

1.9 to 6.5 cm (mean ± std=4.28 ± 0.008 cm, N=74,382), with good focality achieved over dorsolateral prefrontal, temporoparietal, and lateral occipital cortices (Fig. 5A). Electric fields were the least focal for sources on the ventral temporal surface. Stimulation intensity ranged from 0.0002 to 0.50 V/m (mean ± std=0.073 ± 0.075 *V/m*, N=74,382), with discrete "hotspots" appearing on the lateral prefrontal, middle temporal, and occipital cortices (Fig. 5B). Note that the presence of near-zero intensity at some cortical locations indicates that certain areas are simply inaccessible via transcranial stimulation, analogous to "closed-field" configurations in EEG. We also computed the distance between the ground-truth target and the peak of the achieved electric field, terming this the "targeting error". This errorwas less than 1 cm for virtually the entire dorsal surface, while increasing along the ventral surface, sometimes reaching more than 5 cm (Fig. 5C). As expected, a strong and significant negative correlation was observed between focality and intensity ($r = -0.54$, p=0 to numerical precision, N=74,382). Focality was positively correlated with the targeting error (r=0.70), and the targeting error negatively correlated with the intensity ($r = -0.60$).

Reciprocity accounts for source orientation

A leading hypothesis in TES research (at least for direct current stimulation) is that polarization of neurons is dependent on the direction of the applied electric field relative to the affected cells (Rahman et al., 2013). For example, maximal stimulation of pyramidal cells is achieved when the electric field is aligned with the somatodendritic axis (Bikson et al., 2004; Radman et al., 2009). We therefore sought to determine whether the electric fields generated by reciprocal TES are matched to not only the location but also the orientation of the activated sources. To test this, we simulated focal activation of a gyral patch of motor cortex (Fig. 6A) with two source orientations: (i) normal to the local cortical surface and (ii) tangential to the local surface (i.e., front to back). We performed L^1-constrained reciprocal TES ($c = 10^{10}$) for both cases and determined the electric field vector at the activated region. Radial activation led to a largely monopolar EEG pattern over central electrodes (Fig. 6B). Reciprocal stimulation for this scalp topography consisted of two dominant anodes and one dominant cathode (Fig. 6C), and produced an electric field with a strong radial component which was maximal at the source of the radial activation (0.064 V/m, Fig. 6D, activation region indicated by white circle). The field's tangential component at the target location had a weaker intensity (0.0003 V/m, Fig. 6E), meaning that stimulation would have produced significantly more polarization of normally oriented tissue, thus matching the source orientation. Note that the peak of the tangential component of the electric field is no longer at the target location, as the desired field orientation is radial (i.e., the one that matches the activated source). Meanwhile, when the source orientation was tangential, a dipolar pattern centered near the vertex resulted (Fig. 6F). In this case, the anode was positioned anterior of the cathode (Fig. 6G). Importantly, the tangential component of the field was 0.13 V/m (Fig. 6H), while the field strength in the radial direction was only 0.004 V/m (Fig. 6I). Thus, for both radial and tangential activations, the dominant orientation of the reciprocal electric field matched the direction of the activated tissue.

Reciprocal TES with distributed sources

The simulations considered thus far have modeled focal source activations. In order to examine the behavior of reciprocal TES with multiple distributed activations, we

simulated EEG with source nodes in the primary visual cortex (V1), visual area V2, visual area V4, and the inferior temporal cortex (ITC) (Fig. 7A; see Methods for details on activation). These sources roughly correspond to the "ventral visual stream". The EEG pattern emerging from this distributed activation had three areas of focal positivity: one over the medial occipital electrodes, and the other two over bilateral temporal electrodes (Fig. 7B). Reciprocal TES of this pattern consisted of approximately 9 electrodes covering both temporal and occipital locations (Fig. 7C). The ensuing electric field exhibited large magnitudes over the medial occipital cortex, including the visual source regions, and also damped but still pronounced intensity at the site of the inferior temporal activation (Fig. 7D). At the four activated regions, the electric field magnitudes were: 0.13 ± 0.046 V/m (V1), 0.17 ± 0.024 V/m (V2), 0.15 ± 0.012 V/m (V4), 0.066 ± 0.024 V/m (ITC). The lower field intensity at the inferior temporal target relative to the occipital sources was likely due to the general difficulty of reaching ventral targets from the scalp.

Discussion

The duality of TES and EEG

Here we show how measured EEG potentials may be translated into optimal TES montages that generate electric fields focused over the areas of neural activity. To target the sources of observed EEG, we describe a pattern of TES currents matching the *spatially decorrelated* scalp potentials. In contrast, the simplistic strategy of placing the anodes over positive potentials and the cathodes over negative potentials results in drastically suboptimal stimulation (see Fig. 1). Importantly, the determination of the reciprocal TES montage does not require source localizing the measured EEG. However, this does *not* imply that reciprocity has solved the illposed inverse problem of EEG. Rather, it was shown that EEG source localization and TES targeting are in fact two sides of the same optimization problem. Thus, when trying to reciprocate an EEG topography that fails to yield a meaningful source estimate via minimum-norm localization (Sarvas, 1987; Hämäläinen and Ilmoniemi, 1994), the resulting TES targeting "misses" the neural activation (see Fig. 2). In such cases, the peaks of the electric field distribution from reciprocal TES may not be interpreted as the locations of the underlying EEG sources. Therefore, when the available EEG leads to poor reliability of the minimum-norm source estimate, as may be the case for noisy recordings, it may be preferred to guide TES with anatomical as opposed to functional information. Reciprocal TES allows one to stimulate EEG sources using measurements of their activity on the scalp, but with the caveat that the limitations of the targeting mirror those of source localization. Nonetheless, the methods proposed here are numerically optimized given these biophysical constraints. Moreover, our approach prescribes a clear implementation that is applicable to any EEG, while simplifying hardware by minimizing TES electrodes. The approach proposed here is not limited to transcranial stimulation. It applies identically to the case of deep brain stimulation that is guided by electrical recordings of neural activity inside the brain.

The need for a head model

In order to guide TES using EEG, computation of the lead-field matrix R, or equivalently, the forward model S, is required. Without knowledge of how a neural activation projects

to the scalp, or equivalently, how surface TES currents flow in the brain, it is not possible to spatially decorrelate the EEG and thus to target its sources. The complexity of head models ranges from simple concentric-shell BEMs to detailed volumetric FEMs that account for idiosyncratic details (Hallez et al., 2007). It stands to reason that the performance of reciprocal TES will increase with the accuracy (detail) of the head model employed to transform EEG potentials to TES montages. For FEM head models, computation of the lead fields (or forward models) requires solving Laplace's equation across the volume subject to the boundary conditions imposed at the stimulation electrodes (Jackson, 1975). In the approach presented here, the lead fields are computed *a priori* for each linearly independent electrode pair to form the matrix R, which is then employed to target the sources of EEG via (4). Previous approaches to targeting an anatomically defined brain region have solved Laplace's equation as part of the optimization procedure (Wagner et al., 2016a), an approach that may potentially be extended to the case of EEG-guided targeting.

Despite the availability of freely-available tools for constructing forward models (Thielscher et al., 2015; Jung et al., 2013; Truong et al., 2014; SimBio Development Group, 2017), their widespread adoption for designing TES interventions has not transpired. One potential reason for this is the high cost of acquiring structural MRI scans for study participants. In this case, one can opt to use a template head model such as the FEM used here (Mazziotta et al., 1995; Huang et al., 2015). An important question that has not been answered here is how much the performance of reciprocal TES degrades when applying a template model to individualized EEG recordings. It should also be noted that due to reciprocity, lead fields routinely computed for EEG (Tadel et al., 2011; Gramfort et al., 2014) may be equivalently used for TES targeting. One caveat here is that while EEG sources are typically restricted to the grey matter, the target of a TES study may be subcortical. In such cases, however, the EEG is unlikely to be used to inform TES, as the contribution of subcortical areas to the EEG is presumed to be small.

Benefits of L^1-constrained reciprocity

The stimulation currents computed by unconstrained reciprocity (4) may differ in scale from those desired in practice (e.g. 2 mA total). Here we showed that imposing an inequality constraint on the total current led to reciprocal TES montages that adhered to this desired scaling while still focally stimulating the neural sources (see Fig. 3). In fact, L^1-constrained reciprocity produced stimulation that would likely be favored in practice over its unconstrained counterpart: when properly selecting the parameter c, the intensity can be greatly increased while sacrificing only a modest amount of focality (see Fig. 4). The optimal range of c (which models the ratio of intensities between TES electric fields and EEG sources) found here ($10^{10} - 10^{11} \Omega/m^2$) is roughly consistent with present estimates for EEG source intensities (1 nm·A) and TES electric fields (0.5 V/m). In addition to increased intensity, L^1-constrained montages are also more feasible, as they recruit a limited number of electrodes (see Fig. 4). This is a natural consequence of imposing L^1 constraints, which are well-known to yield sparse solutions to least squares problems (Tibshirani, 1996).

Comparison with recent work

The reciprocal TES approach described here leverages EEG recordings. It differs therefore fundamentally from other forms of TES targeting that are based purely on anatomical information (Dmochowski et al., 2011). A previous attempt to leverage EEG for targeting (Cancelli et al., 2016) is based on the intuition that the injected currents should match the recorded voltages ($I \propto V$), which we referred to here as the "naive" reciprocity approach (Figure 1B) as it does not recognize the importance of inverting the blurring introduced by volume conduction. Fernández-Corazza et al. (2016) suggest the use of the traditional reciprocity principle, but fail to recognize the multi-dimensional reciprocity relationship (3). As a result, the EEG and TES problems could not be mathematically synthesized into the least-squares optimization problem developed here (4). Thus, the solutions of Fernández-Corazza et al. (2016) are limited to heuristics relying on individual electrode pairs. Consequently, neither of these two previous efforts were able to focus the electric field onto the site of neural activation. In contrast, the approach presented here is optimal in reproducing the neural source distribution in a least-squares sense.

The common hardware and inherent reciprocity of EEG/TES make this combination attractive for imaging-guided brain stimulation. However, optimization of the TES montage may also be aided by other modalities including fMRI, simultaneous fMRI/EEG (Huster et al., 2012), and simultaneous EEG/MEG (Dale and Sereno, 1993; Aydin et al., 2014). The information provided by these complementary signals may allow one to spatially resolve the target, particularly in the case of a single focal activation. Given a reliable estimate of the target location, approaches that steer the applied currents to that target, such as Dmochowski et al. (2011); Ruffini et al. (2014), or Wagner et al. (2016a), are preferred as they circumvent any ambiguity in target location as inferred from the EEG.

Practical implementation

The EEG is almost always acquired over multiple electrodes and time points, and is thus commonly represented as a space-time data matrix. Reciprocal TES takes as an input a vector of scalp potentials, meaning that the EEG matrix must first be distilled into a time-independent vector. This can be accomplished in several ways. The simplest is to select a time point and use a temporal slice of the data as the input: in this case, the stimulation will be focused on the regions whose activation is strongest during the selected time point. To lessen the sensitivity of the scheme to the particular time point chosen, an alternative approach is to temporally average the EEG across some epoch of the data (e.g. the length of an experimental trial) – in this case, reciprocal TES will target sources most strongly expressed over the epoch duration. Yet another possibility, and one that is most principled, is to decompose the data into spatial components via a technique such as principal components analysis (PCA) (Parra et al., 2005), independent components analysis (ICA) (Delorme and Makeig, 2004), or reliable components analysis (RCA) (Dmochowski et al., 2012, 2015). In this case, one can inspect the topographies of the various components in order to select the one that is to be targeted with reciprocal stimulation. It is important to note that when reciprocating a component of the EEG, one should use the forward projection of the weights and *not* the spatial filter weights themselves (Parra et al., 2005; Haufe et al., 2014).

Physical limits on performance

Given constraints on the number of candidate electrodes (i.e., 230) and the total current delivered (i.e., 2 mA), the maximum achievable focality of reciprocal TES was here found to be approximately 2 cm. As defined here, this means that half of the total electric field was confined to a sphere of 2 cm radius. Fields were most focal across broad areas of lateral cortex, with focality dropping off steeply on the ventral surface (i.e., over 5 cm). Field intensities peaked at 0.5 V/m, with these maximal values located at discrete "hotspots" along dorsal patches of the prefrontal and temporal cortex. These hotspots likely represent locations with a favorable electrical channel from scalp to cortex (and reciprocally, from cortex to scalp). For both focality and intensity, reciprocating sources located along the ventral surface was found to be challenging, with simultaneously low focality and intensity produced by reciprocal TES to those regions.

Implication for closed-loop TES

Closed loop brain stimulation, during which neural recording and stimulation are performed simultaneously or in tandem, has already been shown to be effective in reducing pathophysiological patterns in Parkinson's Disease (Rosin et al., 2011) and blocking epileptic seizures (Berényi et al., 2012; Osorio et al., 2001). In the context of non-invasive techniques, transcranial alternating current stimulation (TACS) has been reported to entrain oscillatory EEG rhythms (for example, alpha oscillations) (Antal and Paulus, 2013), including in an open-loop design taking into account the individual oscillation frequency of the subjects (Zaehle et al., 2010). Unlike these prior techniques, the reciprocal approach developed here uses the spatial (i.e., as opposed to temporal) statistics of neural activity to guide stimulation. As this spatial information is orthogonal to temporal dynamics, our approach may be performed on both oscillatory and evoked activity. Moreover, it could also be combined with existing approaches that tune the temporal frequency of the applied stimulation. While we appear to have a solid understanding of electrical fields generated in the brain during stimulation (Opitz et al., 2016; Huang et al., 2017), it may be argued that we know less about how these electric fields interact with neuronal activity. Closed-loop stimulation efforts will be enhanced by mechanistic knowledge of the micro- and meso-scale interactions between biological activity and the modulating electric fields. In the context of EEG-TES, this entails developing a functional link between the parameters of the stimulation and the resulting changes to the EEG, which is perhaps mediated by the brain state at stimulation onset (Silvanto et al., 2008).

Methods

Here we provide the proofs of the theoretical findings presented in the Results. In particular, by leveraging linear superposition of electric potentials, we derive a vectorial form of the well-known reciprocity between electrical stimulation and recording (Rush and Driscoll, 1969), relating here not a single current source in the volume with a pair of electrodes, but rather an array of electrodes with multiple current sources. We then employ this multidimensional reciprocity to solve for the array of scalp currents that best targets the source of an observed EEG pattern.

Theorem 1. Multi-dimensional reciprocity

$$R^{(i)} = {S^{(i)}}^T, i \in \{x, y, z\}, \tag{9}$$

where $R^{(i)}$ and $S^{(i)}$ denote the ith Cartesian components of the lead-field matrix and forward model, respectively.

Proof. (Theorem 1)—The fundamental reciprocity relation, when written for the case of a single source in the brain and a single electrode pair on the scalp is given by (Rush and Driscoll, 1969):

$$\begin{aligned} V_n I_n &= \mathbf{E}_m \cdot \mathbf{J}_m \\ &= E_m^{(x)} J_m^{(x)} + E_m^{(y)} J_m^{(y)} + E_m^{(z)} J_m^{(z)}, \end{aligned} \tag{10}$$

where V_n is the voltage at scalp location n (relative to a reference electrode) due to a current source $\mathbf{J}_m$ at brain location m (bold font indicates that this is a three-dimensional vector in Cartesian space $\{x, y, z\}$), and reciprocally, $\mathbf{E}_m$ is the electric field vector generated at brain location m when applying a current of I_n to scalp location n (and hence a current of $-I_n$ at the reference electrode). Moreover, we have explicitly written out the x-, y-, and z- components of the electric field as $E_m^{(x)}$, $E_m^{(y)}$, and $E_m^{(z)}$, respectively, with analogous definitions holding for the current source vector $\mathbf{J}_m$.

We seek to extend this result to the case of multiple sources in the brain (indexed by m) and multiple electrode pairs on the scalp (indexed by n). The fundamental observation is that the electric potentials and fields from multiple current sources are additive (Jackson, 1999). Invoking this superposition principle on the component voltages V_{nm} generated at electrode n by multiple brain sources $\mathbf{J}_m$, as given by (10), yields:

$$V_n = \sum_m V_{nm} = \sum_m \frac{\mathbf{E}_{nm} \cdot \mathbf{J}_m}{I_n}, \tag{11}$$

where $\mathbf{E}_{nm}$ is the electric field vector generated at brain location m when stimulating scalp electrode n with intensity I_n. We can express (11) in matrix notation as:

$$\begin{aligned} V &= RJ \\ &= [R^{(x)} \ R^{(y)} \ R^{(z)}] \begin{bmatrix} J^{(x)} \\ J^{(y)} \\ J^{(z)} \end{bmatrix}, \end{aligned} \tag{12}$$

where

$$R_{nm}^{(i)} = E_{nm}^{(i)}/I_n \tag{13}$$

is the element at row n and column m of matrix $R^{(i)}$.

Let us turn now to the stimulation case. We seek to write the net electric field generated in the brain when simultaneously stimulating at multiple scalp electrodes (indexed by n). Once again employing the superposition principle, we write the total electric field as the sum of the individual electric fields generated by stimulation at each electrode:

$$E_m^{(i)} = \sum_n E_{nm}^{(i)}, \tag{14}$$

where $E_m^{(i)}$ is the ith component of the net electric field at brain location m. From (13), we have that $E_{nm}^{(i)} = R_{nm}^{(i)} I_n$, which we substitute into (14) to yield:

$$E_m^{(i)} = \sum_n R_{nm}^{(i)} I_n. \tag{15}$$

Writing (15) in matrix notation leads to:

$$E^{(i)} = {R^{(i)}}^T I, \tag{16}$$

where $E^{(i)}$ is a vector whose mth element is $E_m^{(i)}$, and I is a vector whose nth element is I_n. From (2) and (16), we identify $R^{(i)} = {S^{(i)}}^T$, which is the desired result.

Theorem 2. Reciprocal targeting

In a least-squares sense, the vector of scalp currents I^* which best recreates the neural current source distribution J is given by:

$$I^* = c \left(R R^T \right)^{-1} V. \tag{17}$$

Proof—We seek to minimize the squared error between E and cJ, leading to the following optimization problem:

$$I^* = \arg\ \min_I\ \| E - cJ \|^2. \tag{18}$$

Let distance $D = E - cJ^2$ denote the cost function to be minimized. Taking the derivative with respect to the vector of applied currents I leads to:

$$
\begin{aligned}
\frac{\delta D}{\delta I} &= \frac{\delta}{\delta I} \|E - cJ\|^2 \\
&= \frac{\delta}{\delta I} E^T E - 2c E^T J + c^2 J^T J \\
&= \frac{\delta}{\delta I} (R^T I)^T (R^T I) - 2c (R^T I)^T J + c^2 J^T J \\
&= \frac{\delta}{\delta I} I^T R R^T I - 2c I^T (RJ) + c^2 J^T J \\
&= \frac{\delta}{\delta I} I^T R R^T I - 2c I^T V + c^2 J^T J \\
&= 2 R R^T I - 2c V \,.
\end{aligned}
\tag{19}
$$

Setting (19) to zero leads to

$$
R R^T I = cV,
$$

from which we arrive at the desired result (17).

Reciprocal TES is equivalent to minimum-norm EEG source localization

Here we show that reciprocal TES targeting following (4) is actually the counterpart of the minimum-norm solution to the MEG/EEG source localization problem (Sarvas, 1987; Hämäläinen and Ilmoniemi, 1994). To see this, substitute (4) into (2), yielding the following expression for the electric field generated by reciprocal TES:

$$
E^* = R^T I^* = c R^T (R R^T)^{-1} V \,.
\tag{20}
$$

Consider now the inverse problem of finding the current density distribution J that gave rise to the observed pattern of scalp potentials $V = RJ$. This is an ill-posed problem without a unique solution. A common approach to solving such underdetermined systems is to identify the solution with minimum norm:

$$
J^* = \arg \min_J \|J\|_2 \text{ subject to } V = RJ \,.
\tag{21}
$$

The solution to (21) is given by:

$$
\begin{aligned}
J^* &= R^T (R R^T)^{-1} V \\
&= E^*/c,
\end{aligned}
\tag{22}
$$

where the last line follows from (20).

Algorithm for L[1]-constrained reciprocity

In order to identify the reciprocal TES montage that adheres to a hard constraint on the total current delivered to the head, we seek to solve the following constrained optimization problem:

$$I_1^* = \text{arg } \min_{I} \; \|E - cJ\|^2 \text{ subject to} \|I\|_1 < 2I_{\max} . \quad (23)$$

Following Tibshirani (1996), the non-differentiable L^1 inequality constraint in (23) may be converted into a set of 2^N linear inequality constraints, where N is the number of scalp electrodes:

$$
\begin{aligned}
I_1^* = \text{arg } \min_{I} \; &\|E - cJ\|^2 \text{ subject to} \\
&I_1 + I_2 + \ldots s + I_N < 2I_{\max} \\
&- I_1 + I_2 + \ldots s + I_N < 2I_{\max} \\
&I_1 - I_2 + \ldots s + I_N < 2I_{\max} \\
&\vdots \\
&- I_1 - I_2 - \ldots - I_N < 2I_{\max},
\end{aligned}
\quad (24)
$$

where the linear constraints span all possible "sign" combinations of the current vector I. In principle, the optimization problem (24) may then be solved using conventional quadratic programming. However, for many applications (including this one), the number of linear constraints 2^N is extremely high, making direct implementation of (24) intractable. To circumvent this, Tibshirani also proposed an iterative scheme to solving (24) that begins with the unconstrained solution I^* and proceeds to update the solution, adding a single linear constraint at each iteration (Tibshirani, 1996). Empirical results (including the ones in this paper) show that convergence occurs long before all 2^N constraints have been added to the cumulative set of constraints. In general, the number of iterations required for the algorithm to converge is in the order of N. This efficient iterative scheme was employed here to solve for the L^1-constrained reciprocal TES montage.

Head models

We employed two different head models for this study. The first was a 3-compartment BEM that served to validate the theoretical findings (see Figs. 1–3). The BEM was constructed in the Brainstorm software package (Tadel et al., 2011) for Matlab (Mathworks, Natick, MA). The anatomy of the head was selected as the "ICBM-152" standard, which was constructed by non-linearly averaging 152 individual heads in a common coordinate system (Mazziotta et al., 1995; Fonov et al., 2011). The Brainstorm package relies on the FreeSurfer tool for segmenting the head into its constituent tissue categories (Fischl, 2012). The BEM was constructed with the following (default Brainstorm) parameters: scalp: relative conductivity of 1 S/m, skull: relative conductivity of 0.0125 S/m, brain: relative conductivity of 1 S/m. The model included 15,002 virtual sources (vertices) arranged along the pial surface. 64 scalp electrodes (63 free electrodes + 1 reference) were then placed on the scalp following the international 10/10 standard for EEG. To solve for the lead field from each source to each scalp electrode, Brainstorm employed the Open MEEG tool (Gramfort et al., 2010). This yielded the 63-by-45006 matrix R, where the rows spanned electrodes and the columns spanned the 3 Cartesian orientations of each cortical source.

The second head model, which was used to estimate performance of reciprocal TES in practice (see Figs. 4–7), was a more detailed FEM that captured some of the idiosyncrasies

of the human head. This FEM has been previously described and made publicly available in Huang et al. (2015), and is illustrated in their Fig. 1. We describe here only the key features. The model is based on the ICBM-152 template head (Mazziotta et al., 1995; Fonov et al., 2011), and was manually segmented into six constituent tissue types: scalp, skull, cerebrospinal fluid (CSF), grey matter, white matter, and air cavities. Generation of the tetrahedral meshes was performed at a resolution of 0.5 mm^3. The sources were modeled along the grey matter surface, resulting in a set of 74,382 source nodes. The model included 231 electrodes arranged on the scalp according to an extended 10-5 scheme (Oostenveld and Praamstra, 2001). Note that both here and in the BEM, the electrodes were modeled as individual faces in the tetrahedral meshes (i.e., electrode geometry was not taken into account). The FEM spanned both the head and neck.

When simulating neural activations, the following model was used:

$$V = RJ + W, \tag{25}$$

where W was an $N-1$ element vector of spatially uncorrelated Gaussian noise added to the electrode array. All activated sources had a magnitude of 1 nA m and an orientation perpendicular to the local cortical sheet. Unless otherwise stated, the standard deviation of W was selected to be 0.01 of the standard deviation of RJ (in other words, the nominal SNR was set to 100). It is well-known that in practice, the (single-trial) SNR of EEG data is quite low. Here, however, the SNR was deliberately increased in order to (i) confirm the theoretical findings under low-noise conditions, (ii) because, in practice, reciprocal TES is expected to be applied to either averaged or component data whose SNR is much higher than the single-trial SNR (see Discussion), and (iii) to determine the upper-bounds on performance of reciprocal TES. Neural activations consisted of a "seed" location and a fixed number of vertices K closest to the seed point. The seed location was initially selected by clicking on a vertex on the cortical surface. The value of K was selected (see below for specific values) such that the resulting activation spanned the desired area of cortex.

Unless otherwise indicated, the value of parameter c was set to $10^{10} \Omega/m^2$. All TES montages were restricted to a total current delivered of 2 mA. This was achieved using Eq. (7) for the "optimal" (unconstrained) and "naive" reciprocity, and using Eq. (8) for L^1-constrained reciprocity.

To measure focality, we estimated the radial distance from the target at which the total electric field contained within that radius dropped to half of the total electric field (across all locations). When estimating the number of electrodes recruited by reciprocal TES, we computed the proportion of electrodes carrying at least 5% of the total applied current.

Fig. 1. The seed point was located at (0.038, −0.038, 0.11), and K=25.

Fig. 2. There were two seed points: (−0.028, 0.0083, 0.12) and (−0.025, −0.012, 0.13), each with K= 25.

Fig. 3. For the example activation of visual cortex (Panels A–C), the two seed points (each with K= 25) were located at (−0.070, −0.0084, 0.069) and (−0.070, −0.000018, 0.066).

When simulating activations from all 15,002 sources (Panel D), we iterated over all vertices, each time computing the $K= 50$ vertices closest to the seed vertex. On average, the radius of the minimum sphere which bounded the activated vertices was 1.2 cm.

Fig. 4. The seed location and K values were selected as follows: left superior temporal gyrus (STG) ($-0.070, -0.022, 0.0072$), $K= 80$; left dorsolateral prefrontal cortex (DLPFC) ($-0.038, 0.063, 0.0058$), $K= 80$; left superior parietal lobule: ($-0.028, -0.086, 0.041$), $K= 80$; left middle temporal area (MT): ($-0.057, -0.070, 0.017$), $K= 80$.

Fig. 5. When simulating activations from all 74,382 sources, we iterated over all vertices, each time computing the $K= 40$ vertices closest to the seed vertex. On average, the radius of the minimum sphere which bounded the activated vertices was 0.7 cm.

Fig. 6. The seed point was located at ($-0.035, 0.0051, 0.065$), and $K=20$. The orientation of the tangential source was set to $(0, 1, 0)$.

Fig. 7. The seed points, K values, and source intensities were selected as follows: V1 ($-0.0078, -0.10, 0.0028$) and ($-0.0078, -0.10, 0.0028$) with $K=40$ each and intensity of 1 nm·A; V2 ($-0.021, -0.10, 0.0047$) and ($0.021, -0.10, 0.0047$) with $K=40$ each and intensity of 1 nm·A; V4 ($-0.026, 0.10, -0.0048$) and ($0.026, -0.10, -0.0048$) with $K=40$ each and intensity of 1 nm·A; ITC ($-0.062, -0.035, -0.028$) and ($0.062, -0.035, -0.028$) with $K=80$ each and intensity of 4 nm·A. The intensities of the sources in ITC were chosen such that their projection to the scalp had equivalent power as the occipital sources.

Public availability of data

The head model, as well as the code to perform reciprocal TES, are available for download in Matlab format at: http://www.jd-lab.org/resources.

References

Antal A, Paulus W. 2013 Transcranial alternating current stimulation (tacs). Front Human Neurosci. :7.

Aydin Ü, Vorwerk J, Küpper P, Heers M, Kugel H, Galka A, Hamid L, Wellmer J, Kellinghaus C, Rampp S, et al. 2014; Combining eeg and meg for the reconstruction of epileptic activity using a calibrated realistic volume conductor model. PLoS One. 9 (3) :e93154. [PubMed: 24671208]

Berényi A, Belluscio M, Mao D, Buzsáki G. 2012; Closed-loop control of epilepsy by transcranial electrical stimulation. Science. 337 (6095) :735–737. [PubMed: 22879515]

Bergmann TO, Karabanov A, Hartwigsen G, Thielscher A, Siebner HR. 2016 Combining non-invasive transcranial brain stimulation with neuroimaging and electrophysiology: Current approaches and future perspectives. NeuroImage.

Bestmann S, Feredoes E. 2013; Combined neurostimulation and neuroimaging in cognitive neuroscience: past, present, and future. Ann N Y Acad Sci. 1296 (1) :11–30. [PubMed: 23631540]

Bikson M, Grossman P, Thomas C, Zannou AL, Jiang J, Adnan T, Mourdoukoutas AP, Kronberg G, Truong D, Boggio P, et al. 2016; Safety of transcranial direct current stimulation: evidence based update 2016. Brain Stimul. 9 (5) :641–661. [PubMed: 27372845]

Bikson M, Inoue M, Akiyama H, Deans JK, Fox JE, Miyakawa H, Jefferys JG. 2004; Effects of uniform extracellular dc electric fields on excitability in rat hippocampal slices in vitro. J Physiol. 557 (1) :175–190. [PubMed: 14978199]

Brunoni AR, Nitsche MA, Bolognini N, Bikson M, Wagner T, Merabet L, Edwards DJ, Valero-Cabre A, Rotenberg A, Pascual-Leone A, et al. 2012; Clinical research with transcranial direct current

stimulation (tdcs): challenges and future directions. Brain Stimul. 5 (3) :175–195. [PubMed: 22037126]

Cancelli A, Cottone C, Tecchio F, Truong DQ, Dmochowski J, Bikson M. 2016; A simple method for eeg guided transcranial electrical stimulation without models. J Neural Eng. 13 (3) :036022. [PubMed: 27172063]

Dale AM, Sereno MI. 1993; Improved localizadon of cortical activity by combining eeg and meg with mri cortical surface reconstruction: a linear approach. J Cogn Neurosci. 5 (2) :162–176. [PubMed: 23972151]

Delorme A, Makeig S. 2004; EEGLAB: an open source toolbox for analysis of single-trial EEG dynamics including independent component analysis. J Neurosci Methods. 134 (1) :9–21. [PubMed: 15102499]

Dmochowski JP, Datta A, Bikson M, Su Y, Parra LC. 2011; Optimized multi-electrode stimulation increases focality and intensity at target. J Neural Eng. 8 (4) :046011. [PubMed: 21659696]

Dmochowski JP, Greaves AS, Norcia AM. 2015; Maximally reliable spatial filtering of steady state visual evoked potentials. Neuroimage. 109 :63–72. [PubMed: 25579449]

Dmochowski JP, Sajda P, Dias J, Parra LC. 2012; Correlated components of ongoing eeg point to emotionally laden attention-a possible marker of engagement? Front Hum Neurosci. 6 :112. [PubMed: 22623915]

Dostrovsky J, Levy R, Wu J, Hutchison W, Tasker R, Lozano A. 2000; Microstimulation-induced inhibition of neuronal firing in human globus pallidus. J Neurophysiol. 84 (1) :570–574. [PubMed: 10899228]

Faria P, Fregni F, Sebastião F, Dias AI, Leal A. 2012; Feasibility of focal transcranial dc polarization with simultaneous eeg recording: preliminary assessment in healthy subjects and human epilepsy. Epilepsy Behav. 25 (3) :417–425. [PubMed: 23123281]

Fernández-Corazza M, Turovets S, Luu P, Anderson E, Tucker D. 2016; Transcranial electrical neuromodulation based on the reciprocity principle front. Psychiatry. 7 :87.

Fischl B. 2012; Freesurfer. Neuroimage. 62 (2) :774–781. [PubMed: 22248573]

Fonov V, Evans AC, Botteron K, Almli CR, McKinstry RC, Collins DL, Group BDC, et al. 2011; Unbiased average age-appropriate atlases for pediatric studies. NeuroImage. 54 (1) :313–327. [PubMed: 20656036]

Gramfort A, Luessi M, Larson E, Engemann DA, Strohmeier D, Brodbeck C, Parkkonen L, Hämäläinen MS. 2014; MNE software for processing MEG and EEG data. Neuroimage. 86 :446–460. [PubMed: 24161808]

Gramfort A, Papadopoulo T, Olivi E, Clerc M. 2010; Openmeeg: opensource software for quasistatic bioelectromagnetics. Biomed Eng Online. 9 (1) :1. [PubMed: 20051137]

Guggenmos DJ. 2013; Restoration of function after brain damage using a neural prosthesis. Proc Natl Acad Sci. 110 (52) :21177–21182. [PubMed: 24324155]

Hallez H, Vanrumste B, Grech R, Muscat J, De Clercq W, Vergult A, D'Asseler Y, Camilleri KP, Fabri SG, Van Huffel S, et al. 2007; Review on solving the forward problem in eeg source analysis. J Neuroeng Rehabil. 4 (1) :1. [PubMed: 17244363]

Hämäläinen MS, Ilmoniemi RJ. 1994; Interpreting magnetic fields of the brain: minimum norm estimates. Med Biol Eng Comput. 32 (1) :35–42. [PubMed: 8182960]

Haufe S, Meinecke F, Görgen K, Dähne S, Haynes JD, Blankertz B, Bießmann F. 2014; On the interpretation of weight vectors of linear models in multivariate neuroimaging. Neuroimage. 87 :96–110. [PubMed: 24239590]

Helmholtz, Hv. 1853; Ueber einige gesetze der vertheilung elektrischer ströme in körperlichen leitern, mit anwendung auf die thierisch-elektrischen versuche (schluss.) Ann der Phys. 165 (7) :353–377.

Huang Y, Liu AA, Lafon B, Friedman D, Dayan M, Wang X, Bikson M, Doyle WK, Devinsky O, Parra LC. 2017; Measurements and models of electric fields in the in vivo human brain during transcranial electric stimulation. eLife. 6 :e18834. [PubMed: 28169833]

Huang Y, Parra LC, Haufe S. 2015 The new york head–a precise standardized volume conductor model for eeg source localization and tes targeting. NeuroImage.

Huster RJ, Debener S, Eichele T, Herrmann CS. 2012; Methods for simultaneous EEG-fMRI: an introductory review. J Neurosci. 32 (18) :6053–6060. [PubMed: 22553012]

Jackson, JD. Electrodynamics. Wiley Online Library; 1975.

Jackson, JD. Classical Electrodynamics. Wiley; 1999.

Jimbo Y, Kasai N, Torimitsu K, Tateno T, Robinson HP. 2003; A system for mea-based multisite stimulation. Biomed Eng IEEE Trans. 50 (2) :241–248.

Jung YJ, Kim JH, Im CH. 2013; Comets: a matlab toolbox for simulating local electric fields generated by transcranial direct current stimulation (tdcs). Biomed Eng Lett. 3 (1) :39–46.

Kent AR, Grill WM. 2013; Neural origin of evoked potentials during thalamic deep brain stimulation. J Neurophysiol. 110 (4) :826–843. [PubMed: 23719207]

Lempka SF, McIntyre CC. 2013; Theoretical analysis of the local field potential in deep brain stimulation applications. PLoS One. 8 (3) :e59839. [PubMed: 23555799]

Maynard EM, Nordhausen CT, Normann RA. 1997; The utah intracortical electrode array: a recording structure for potential brain-computer interfaces. Electroencephalogr Clin Neurophysiol. 102 (3) :228–239. [PubMed: 9129578]

Mazziotta JC, Toga AW, Evans A, Fox P, Lancaster J. 1995; A probabilistic atlas of the human brain: theory and rationale for its development: the international consortium for brain mapping (icbm). Neuroimage. 2 (2) :89–101. [PubMed: 9343592]

Nunez, PL, Srinivasan, R. Electric Fields of the Brain: the Neurophysics of EEG. Oxford University Press; USA: 2006.

Oostenveld R, Praamstra P. 2001; The five percent electrode system for highresolution EEG and ERP measurements. Clin Neurophysiol. 112 (4) :713–719. [PubMed: 11275545]

Opitz A, Falchier A, Yan C-G, Yeagle E, Linn G, Megevand P, Thielscher A, Milham M, Mehta A, Schroeder C. 2016 Spatiotemporal structure of intracranial electric fields induced by transcranial electric stimulation in human and nonhuman primates. bioRxiv. :053892.

Osorio I, Frei MG, Manly BF, Sunderam S, Bhavaraju NC, Wilkinson SB. 2001; An introduction to contingent (closed-loop) brain electrical stimulation for seizure blockage, to ultra-short-term clinical trials, and to multidimensional statistical analysis of therapeutic efficacy. J Clin Neurophysiol. 18 (6) :533–544. [PubMed: 11779966]

Parra LC, Spence CD, Gerson AD, Sajda P. 2005; Recipes for the linear analysis of eeg. Neuroimage. 28 (2) :326–341. [PubMed: 16084117]

Pascual-Marqui RD. 1999; Review of methods for solving the eeg inverse problem. Int J Bioelectromagn. 1 (1) :75–86.

Radman T, Ramos RL, Brumberg JC, Bikson M. 2009; Role of cortical cell type and morphology in subthreshold and suprathreshold uniform electric field stimulation in vitro. Brain Stimul. 2 (4) :215–228. [PubMed: 20161507]

Rahman A, Reato D, Arlotti M, Gasca F, Datta A, Parra LC, Bikson M. 2013; Cellular effects of acute direct current stimulation: somatic and synaptic terminal effects. J Physiol. 591 (10) :2563–2578. [PubMed: 23478132]

Rosenberg D, Mauguiere F, Catenoix H, Faillenot I, Magnin M. 2009; Reciprocal thalamocortical connectivity of the medial pulvinar: a depth stimulation and evoked potential study in human brain. Cereb Cortex. 19 (6) :1462–1473. [PubMed: 18936272]

Rosin B, Slovik M, Mitelman R, Rivlin-Etzion M, Haber SN, Israel Z, Vaadia E, Bergman H. 2011; Closed-loop deep brain stimulation is superior in ameliorating parkinsonism. Neuron. 72 (2) :370–384. [PubMed: 22017994]

Ruffini G, Fox MD, Ripolles O, Miranda PC, Pascual-Leone A. 2014; Optimization of multifocal transcranial current stimulation for weighted cortical pattern targeting from realistic modeling of electric fields. Neuroimage. 89 :216–225. [PubMed: 24345389]

Rush S, Driscoll DA. 1969; Eeg electrode sensitivity-an application of reciprocity. Biomed Eng IEEE Trans. 1 :15–22.

Sarvas J. 1987; Basic mathematical and electromagnetic concepts of the biomagnetic inverse problem. Phys Med Biol. 32 (1) :11. [PubMed: 3823129]

Siebner HR, Bergmann TO, Bestmann S, Massimini M, Johansen-Berg H, Mochizuki H, Bohning DE, Boorman ED, Groppa S, Miniussi C, et al. 2009; Consensus paper: combining transcranial stimulation with neuroimaging. Brain Stimul. 2 (2) :58–80. [PubMed: 20633405]

Silvanto J, Muggleton N, Walsh V. 2008; State-dependency in brain stimulation studies of perception and cognition. Trends Cogn Sci. 12 (12) :447–454. [PubMed: 18951833]

SimBio Development Group. [Accessed 10 May] SimBio: A generic environment for bio-numerical simulations. 2017. online, ⟨https://www.mrt.uni-jena.de/simbio⟩

Tadel F, Baillet S, Mosher JC, Pantazis D, Leahy RM. 2011; Brainstorm: a user-friendly application for meg/eeg analysis. Comput Intell Neurosci. 2011 :8.

Thielscher, A; Antunes, A; Saturnino, GB. Field modeling for transcranial magnetic stimulation: A useful tool to understand the physiological effects of tms? In 2015. Proceedings of the 37th Annual International Conference of the IEEE Engineering in Medicine and Biology Society (EMBC); IEEE; 2015. 222–225.

Thut G, Ives JR, Kampmann F, Pastor MA, Pascual-Leone A. 2005; A new device and protocol for combining tms and online recordings of eeg and evoked potentials. J Neurosci Methods. 141 (2) :207–217. [PubMed: 15661302]

Tibshirani R. 1996 Regression shrinkage and selection via the lasso. Journal of the Royal Statistical Society Ser B (Methodol). :267–288.

Trebuchon A, Guye M, Tcherniack V, Tramoni E, Bruder N, Metellus P. 2012; interest of eeg recording during direct electrical stimulation for brain mapping function in surgery. Ann Fr D'Anesth Et De Reanim. 31 (6) :e87–90.

Truong DQ, Hüber M, Xie X, Datta A, Rahman A, Parra LC, Dmochowski JP, Bikson M. 2014; Clinician accessible tools for gui computational models of transcranial electrical stimulation: bonsai and spheres. Brain Stimul. 7 (4) :521–524. [PubMed: 24776786]

Uhlhaas PJ, Singer W. 2006; Neural synchrony in brain disorders: relevance for cognitive dysfunctions and pathophysiology. Neuron. 52 (1) :155–168. [PubMed: 17015233]

Uhlhaas PJ, Singer W. 2012; Neuronal dynamics and neuropsychiatric disorders: toward a translational paradigm for dysfunctional large-scale networks. Neuron. 75 (6) :963–980. [PubMed: 22998866]

Wagner S, Burger M, Wolters CH. 2016a; An optimization approach for well-targeted transcranial direct current stimulation. SIAM J Appl Math. 76 (6) :2154–2174.

Wagner S, et al. 2016b Using reciprocity for relating the simulation of transcranial current stimulation to the EEG forward problem. NeuroImage.

Zaehle T, Rach S, Herrmann CS. 2010; Transcranial alternating current stimulation enhances individual alpha activity in human eeg. PLoS One. 5 (11) :e13766. [PubMed: 21072168]
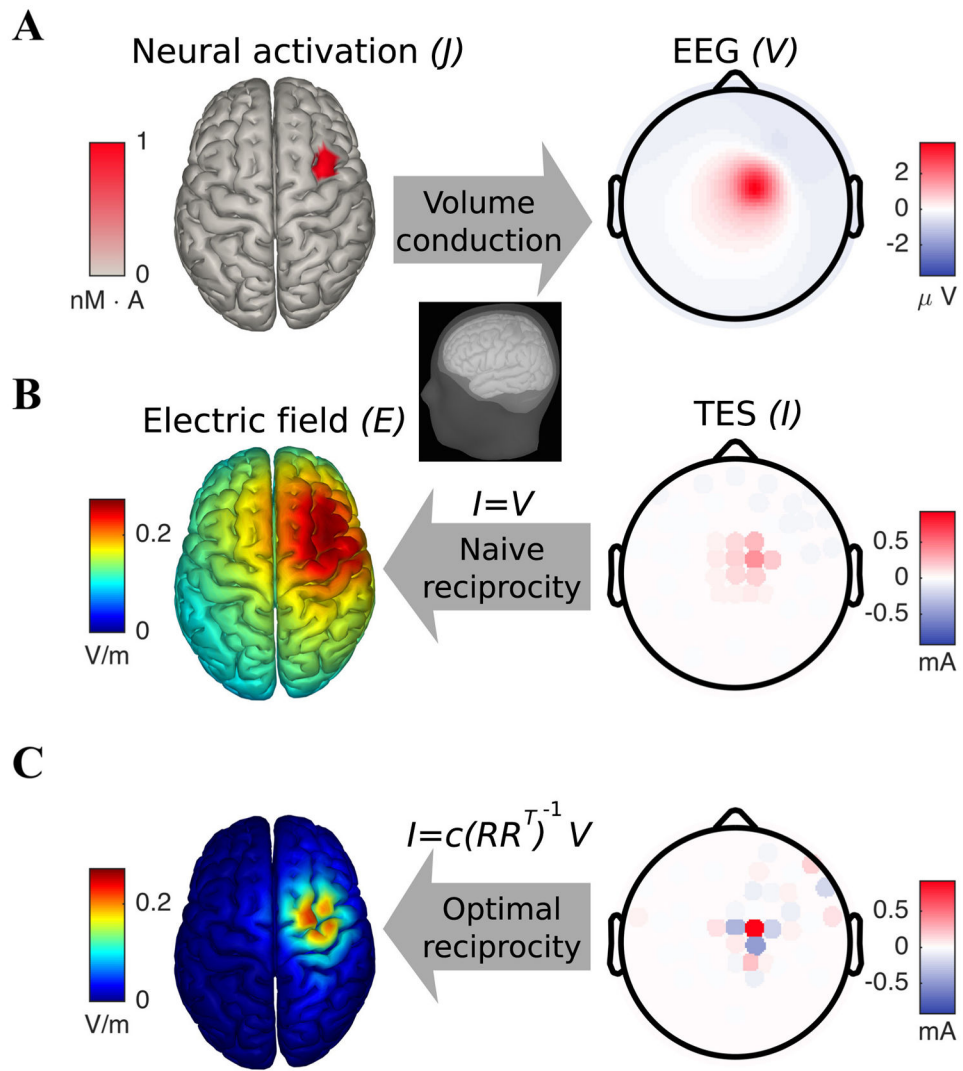
Fig. 1.
Reciprocal stimulation produces an electric field focused on the site of neural activation.
(A) Focal neural activation of the right frontocentral cortex produces a radially-symmetric pattern of electric potentials on the scalp. Inset: BEM head model employed to simulate EEG activations and electric fields during TES. **(B)** By patterning the stimulation currents according to the observed scalp activity (i.e., $I \propto V$), "naive" reciprocity generates a diffuse electric field that is strong at the site of activation but also over expansive regions of cortex. **(C)** Applying TES in proportion to the spatially decorrelated EEG (i.e., $I = c(RR^T)^{-1} V$) yields focal stimulation at the neural activation. Note that the injected reciprocal currents are both positive ("anodal") and negative ("cathodal") over the scalp regions marked by positive EEG potentials.
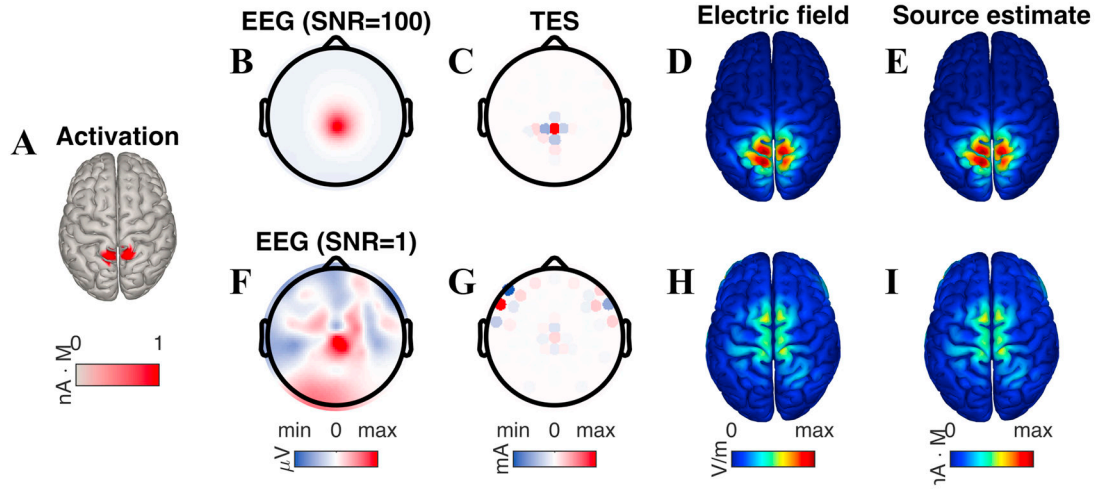
Fig. 2.
Localization of EEG is equivalent to targeting in TES. **(A)** Bilateral activation of the superior parietal lobule. **(B)** The observed EEG pattern, simulated here for a high signal-to-noise ratio (SNR) of 100, shows a radially-symmetric topography focused over centroparietal electrodes. **(C)** The TES montage that targets the source of this EEG is composed of a center anode and surrounding cathodes, producing an electric field **(D)** concentrated at the source of the parietal activation. Moreover, this electric field is perfectly correlated with the minimum-norm estimate **(E)** of the EEG source distribution. **(F)** An increase in the noise level (SNR=1) leads to a distorted EEG topography, which then results in a reciprocal TES montage **(G)** that erroneously utilizes lateral frontal electrodes. The resulting electric field **(H)** is no longer focused on the site of neural activation. Correspondingly, the estimate of the EEG source **(I)** is also mismatched with the actual neural activation.
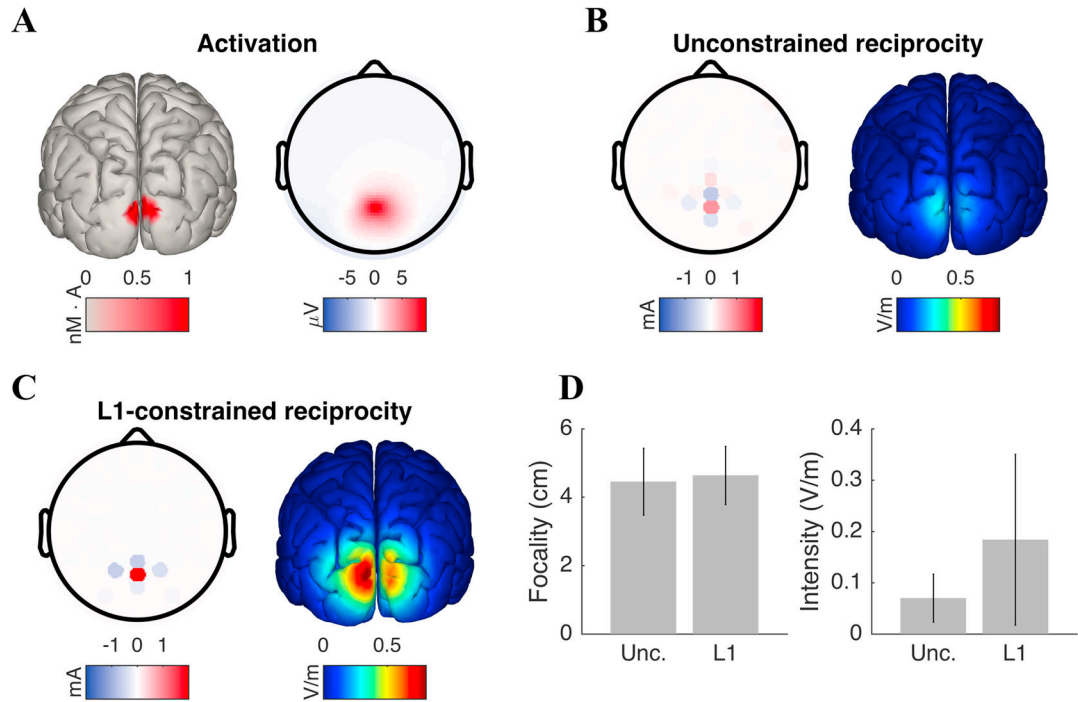
Fig. 3.

Constraining the L^1 norm of reciprocal TES montages produces intense electric fields at the target. **(A)** Activation of primary visual cortex and the associated EEG pattern. **(B)** Unconstrained reciprocity distributed the applied current over approximately 8 electrodes. This led to a concentration of the electric field at the occipital target (focality of 3.3 cm), with a peak electric field intensity of 0.18 V/m. **(C)** By constraining the L^1-norm of the reciprocal TES solution with $c = 10^{10}$, the applied currents were contained to 5 electrodes, yielding to a three-fold increase in the intensity of the stimulation at the activated region (0.53 V/m), while only sacrificing 4 mm in focality (3.7 cm). **(D)** Comparing unconstrained and L^1-constrained reciprocity across all cortical sources showed that L^1-constrained reciprocity achieves an average increase in field intensity of 163%, while only sacrificing 4% in focality (error bars represent standard deviations across 15,002 sources).
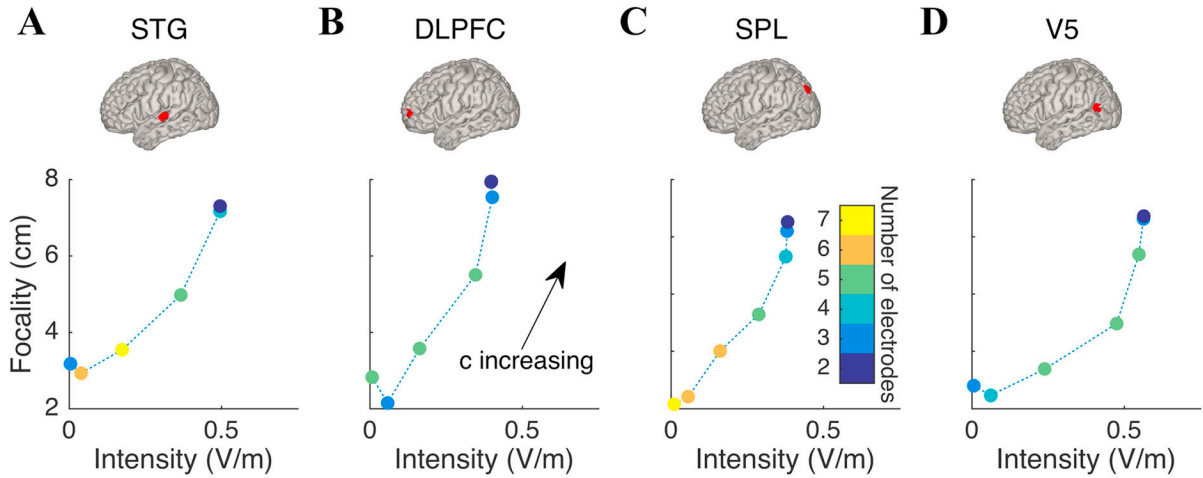
Fig. 4.
Quantifying the focality-intensity tradeoff in L^1 constrained reciprocity. L^1 constrained reciprocal TES at increasing values of parameter c was performed on the EEG generated by activation of the (**A**) superior temporal gyrus (STG), (**B**) the dorsolateral prefrontal cortex (DLPFC), (**C**) superior parietal lobule (SPL) and (**D**) visual area V5 (also known as the middle temporal visual area). Increasing c led to higher intensity and reduced focality at the activation. However, the focality-intensity increased gradually at low values of c, suggesting that intensity can be significantly increased (2 or 3×) while only sacrificing a small amount of focality (1 or 2 cm). A good tradeoff between intensity and focality was found here to be $c = 10^{10}$ or $c = 10^{11}$. Increasing c also led to a reduction in the number of electrodes recruited by the optimal montage (denoted by color of markers), which was approximately 4–7 at $c = 10^{10}$.
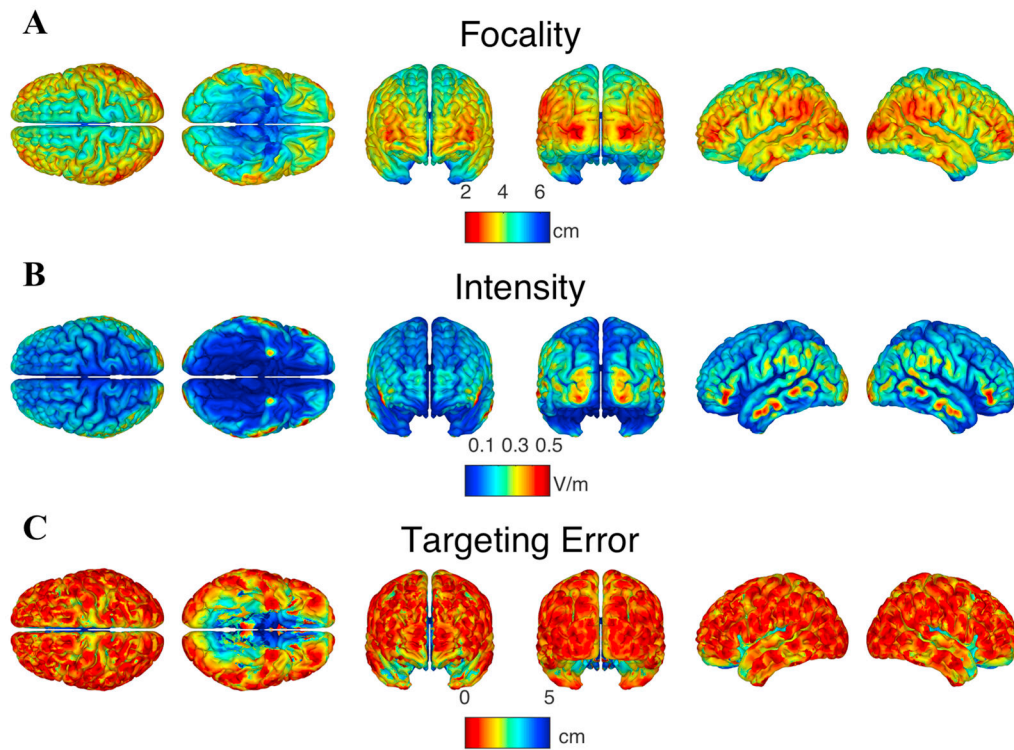
Fig. 5.

The performance of reciprocal stimulation as a function of target location. **(A)** The focality of L^1-constrained reciprocal TES, as measured by the radius bounding half of the total electric field, shown as a function of the location of neural activation. Focality ranged from 1.9 to 6.5 cm, exhibiting optimal values over dorsolateral prefrontal, temporoparietal, and lateral occipital cortices. **(B)** Same as A but now for the intensity of the electric field at the target. Intensity ranged from 0.0002 to 0.50 V/m, exhibiting discrete hotspots over lateral prefrontal, middle temporal, and occipital cortex. **(C)** The error between target location and the peak of the electric field was less than 1 cm along the dorsal surface, while exceeding 5 cm on ventral cortex. The three measures were all significantly correlated ($|t| > 0.56$, $p=0$ to numerical precision, $N=74382$), with locations receiving focal stimulation stimulated with high intensity and low targeting error.
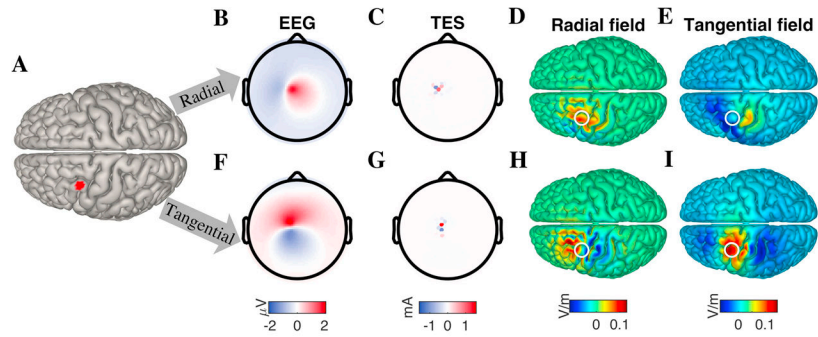
Fig. 6.

Reciprocal TES accounts for varying source orientation. (**A**) A source in the left motor cortex was activated with both radial and tangential source orientations. (**B**) Radial activation led to a monopolar EEG pattern over central electrodes. (**C**) The reciprocal TES montage for this scalp pattern consisted of two dominant anodes and one dominant cathode. (**D**) The resulting electric field was marked by a strong radial component (0.064 V/m) and a significantly weaker (**E**) tangential component (0.0003 V/m) at the intended source location (white circle). Note that the peak of the tangential field is no longer over the target, as the source is *radially* oriented. (**F**) Activation of a *tangential* source at the same target location resulted in a dipolar pattern of scalp potentials. (**G**) The TES montage targeting this EEG pattern consisted of a single dominant anode and cathode. (**H**) This montage produced a weak radial electric field component (0.004 V/m) relative to the (**I**) tangential direction of the electric field (0.13 V/m). Thus, for both cases, reciprocal TES produced an electric field whose dominant direction matched the orientation of the activated source. Note that projections of the electric field in the radial or tangential direction may be positive or negative.
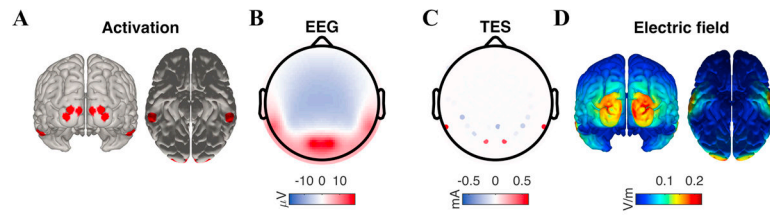
Fig. 7.
Reciprocal TES with distributed source activations. (**A**) Activation of distinct regions along the ventral visual stream (from middle out): primary visual cortex (V1), V2, V4, and the inferior temporal cortex (ITC). (**B**) The resulting EEG pattern showed focal positivity over the bilateral temporal and medial occipital electrodes. (**C**) Reciprocal TES on this EEG pattern led to a montage with stimulation electrodes positioned at both occipital and temporal sites. (**D**) The resulting electric field had pronounced intensity at both occipital and inferior temporal targets. However, the strength of the field was dampened at the inferior temporal sources (0.066 V/m) relative to that at the occipital sources (>0.12 V/m), presumably reflecting the difficulty in targeting ventral regions with TES.